Growth and aging in a few phase-separating active matter systems

Florian Dittrich,[1] Jiarul Midya,[2,3] Peter Virnau,[1,*] and Subir K. Das[4,†]
[1]*Institute of Physics, Johannes Gutenberg University Mainz, 55128 Mainz, Germany*
[2]*Theoretical Physics of Living Matter, Forschungszentrum Jülich, 52425 Jülich, Germany*
[3]*School of Basic Sciences, Indian Institute of Technology, Bhubaneswar 752050, India*
[4]*Theoretical Sciences Unit and School of Advanced Materials, Jawaharlal Nehru Centre for Advanced Scientific Research, Jakkur P.O., Bangalore 560064, India*

(Received 12 December 2022; accepted 22 July 2023; published 21 August 2023)

Via computer simulations we study evolution dynamics in systems of continuously moving active Brownian particles. The obtained results are discussed against those from the passive 2D Ising case. Following sudden quenches of random configurations to state points lying within the miscibility gaps and to the critical points, we investigate the far-from-steady-state dynamics by calculating quantities associated with structure and characteristic length scales. We also study aging for quenches into the miscibility gap and provide a quantitative picture for the scaling behavior of the two-time order-parameter correlation function. The overall structure and dynamics are consistent with expectations from the Ising model. This remains true for certain active lattice models as well, for which we present results for quenches to the critical points.

DOI: 10.1103/PhysRevE.108.024609

I. INTRODUCTION

Nonequilibrium models of self-propelled or active particles describe a multitude of phenomena ranging from the movement of bacteria and artifical microswimmers to macroscopic flocks of birds [1–3]. Some of these systems exhibit cooperative phenomena such as motility-induced phase separation (MIPS) [4] that resembles the passive liquid-gas phase separation but occurs in absence of any attractive interactions: At large propulsion speeds and low rotational diffusion, artificial microswimmers can self-trap and form clusters. The resulting phase diagram shows a binodal curve of coexisting densities that ends in a critical point. Computationally, artificial microswimmers are often studied with continuously moving active Brownian particles (ABPs) [5–13] or variants thereof, but recently active lattice models have gained attention as well [14–16].

Whether the phase behavior in the vicinity of a nonequilibrium critical point is unique, and if it belongs to any standard universality class is a question of fundamental interest and has sparked an ongoing controversy [15–22]. For ABPs, a determination of the critical point and its associated critical exponents revealed results incompatible with any known universality class [17], while active Ornstein-Uhlenbeck particles appear to be compatible with 2D-Ising behavior [19,21,22]. Similarly, active lattice models exhibit exponents close to the 2D-Ising values [15] even though small model-dependant deviations remain [16]. For the description of static critical behavior first theoretical approaches have appeared recently which may reconcile some of these discrepancies [18,20].

In this manuscript we focus on dynamical aspects of active systems. Understanding of nonequilibrium dynamics following quenches of homogeneous systems to the critical point, as well as to state points inside the coexistence region, is of fundamental as well as practical relevance [23,24]. In the context of passive matter systems associated phenomena received much attention. In this broad area, recent focus has been on active matter systems [25–31]. In a class of studies the objective is to understand the scaling behaviors related to structure, growth, and aging [23,26,32–36]. Below we provide brief descriptions of these nonequilibrium aspects.

Typically, growth in such nonequilibrium situations, following quenches inside the coexistence region, occurs in a power-law fashion, viz., average size of domains, rich or poor in particles of a particular type, ℓ, grows with time (t) as [23]

$$\ell \sim t^{\alpha}. \tag{1}$$

Such a growth is usually self-similar in nature, i.e., the domain patterns at two different times are different from each other only via a change in ℓ. This property is reflected in the scaling behavior of the two-point equal time correlation function [23],

$$C(r,t) = \langle \psi(\vec{r},t)\psi(0,t)\rangle - \langle \psi(\vec{r},t)\rangle\langle \psi(0,t)\rangle, \tag{2}$$

as [23]

$$C(r,t) \equiv \tilde{C}(r/\ell). \tag{3}$$

Here ψ is a space- ($\vec{r}$) and time-dependent order parameter. Another important property associated with such nonequilibrium systems is the aging phenomena. This can be captured in the relaxation behavior of the two-time order-parameter auto-correlation function [32]

$$C_{\rm ag}(t,t_w) = \langle \psi(\vec{r},t)\psi(\vec{r},t_w)\rangle - \langle \psi(\vec{r},t)\rangle\langle \psi(\vec{r},t_w)\rangle, \tag{4}$$

*virnau@uni-mainz.de
†das@jncasr.ac.in

where t_w ($< t$) is a waiting time, also referred to as the age of the system. As opposed to the equilibrium systems, the time translation invariance in growing systems is not obeyed. Note that the rate of relaxation is expected to be different for different ages of a system. Thus, C_{ag} does not exhibit collapse of data from different values of t_w when plotted versus $t - t_w$, but is reported to exhibit collapse when plotted as a function of t/t_w [32], with the scaling form

$$C_{ag} \sim \left(\frac{t}{t_w}\right)^{-\alpha\lambda}, \tag{5}$$

λ being referred to as an aging exponent. With the increase of the exponent λ, the decay of $C(t, t_w)$ becomes generally faster. In the domain of kinetics of phase transitions, λ is a key quantity for the determination of the universality classes.

Similar interest exists for quenches to the critical point. In this case the correlation in the system is expected to grow with time as [29,37,38]

$$\xi(t) \sim t^{1/z}, \tag{6}$$

z being a dynamic critical exponent. Note that in the long time limit values of ξ diverge with the approach to the critical point in a power-law fashion with an exponent ν [39].

Obtaining the values of α, λ, and z are of fundamental importance in the domain of dynamics of phase transitions. Understanding of these are quite advanced for various lattice systems in the case of passive matter. For fluids, the status is reasonably poor. In the case of active matter systems, such interest is very recent. In this work, we intend to obtain these quantities for phase-separating systems consisting of active Brownian particles [4,17]. In addition, we also study active lattice systems [14,15] as they are computationally less demanding and thus yield statistically better data. These systems did show interesting deviations in steady-state critical behavior from ABPs in prior work [16]. Therefore, a comparative analysis of dynamical behavior adds further understanding toward the uniqueness of active matter systems.

Note that self-propelled particles forming nonequilibrium active systems offer a wide range of interesting behavior and applications [1–3,40,41]. While phase transition and the overall nonequilibrium behavior in these systems constitute a broad field of ongoing research [5–12,17], we add an additional aspect of nonequilibrium behavior by quenching uncorrelated homogeneous active systems to correlated or phase separated states.

II. METHODS

A. Model and simulations: Active Brownian particles

Systems of active Brownian particles in two dimensions consist of hard disks which are actively propelled along their orientation (see below). Periodic boundary conditions are applied in both dimensions and equations of motion are given by [17]

$$\dot{\mathbf{r}}_k = -\frac{D_t}{k_B T}\nabla_k U + v_0\begin{pmatrix}\cos\varphi_k\\ \sin\varphi_k\end{pmatrix} + \sqrt{2D_t}\mathbf{R}_k, \tag{7}$$

where $\mathbf{R}_k$ is normal distributed Gaussian noise, D_t the translational diffusion constant, and U arises from a purely repulsive Weeks-Chandler-Andersen (WCA) potential between disks with $\epsilon = 100$ and $\sigma = 1$ as in Ref. [17]. If not mentioned otherwise, then units are from now on omitted and correspond to standard simulation units. Furthermore, D_t is set to 1. With a cutoff distance of $r = 2^{1/6}$ we obtain an effective hard disk Barker-Henderson diameter $d_{\mathrm{BH}} \approx 1.10688$. A particle's orientation is described by the angle φ_k, which undergoes free rotational diffusion with diffusion coefficient D_r, i.e. $\dot{\varphi}_k = \sqrt{2D_r}R_r$, where R_r is Gaussian distributed, has unit variance and is neither correlated between particles nor in time. Each particle is propelled along its orientation with constant speed v_0. GPU-based simulations were performed using HOOMD-blue [42] applying a Brownian integrator with a time step of 10^{-6}. Temperature was set to 1, and simulations were performed at fixed volumes and particle numbers. If the rotational diffusion D_r (set to $3D_t/d_{\mathrm{BH}}^2 \approx 2.45$ throughout this work) is small with respect to the active velocity v_0, then a self-trapping mechanism can be observed [4,43]. Particles that form an emerging cluster require more time to orient away from the cluster than it takes for other particles to reach and enlarge it. This leads to a separation into a dense and a dilute phase and a nonequilibrium phase diagram with a critical point (Fig. 1) [17] even in the absence of explicit attractions.

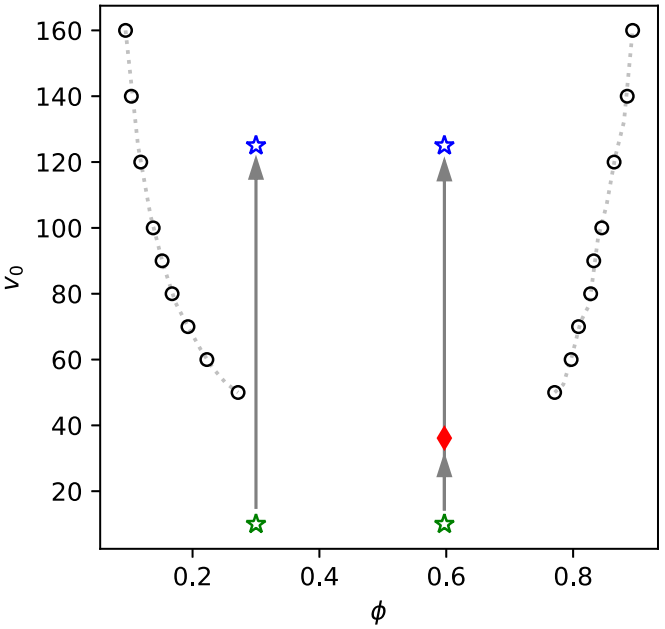

FIG. 1. Phase diagram for ABPs as shown in Ref. [17]. The green stars at the bottom mark the initialization points from where the systems were quenched at constant packing fractions $\phi = 0.597$ and $\phi = 0.3$ into the phase separated region (blue stars at the top) and to the critical point (red diamond). Dotted lines were only drawn to guide the eye.

In the present work we have performed several quenches into the phase-separated region and to the critical point. All simulations started in a mixed state with $v_0 = 10$ and were first equilibrated for 2×10^7 time steps (corresponding to 20 MD times). For the quenches into the phase-separated region the final active velocity was set to $v_0 = 125$. Critical density ($\phi = 0.597$ [17]) was established in a system of size 1024×1024 with 649 636 particles [Fig. 2(b)], while the quench to the low-density branch (at $\phi = 0.3$) [Fig. 2(a)]

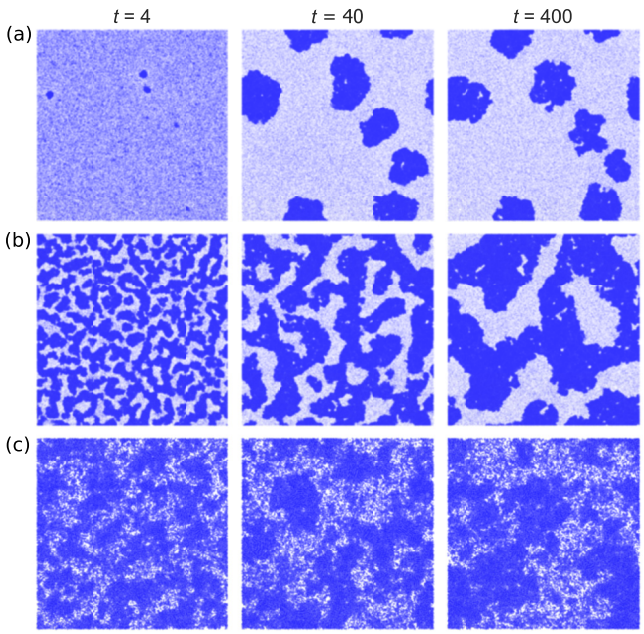

FIG. 2. Snapshots obtained during the evolutions of the ABP model, at three different times, after the quenches took place. Time t is given in MD units. (a) For density $\phi = 0.3$, we have simulated system size 1024×1024 following quench to $v_0 = 125$. (b) For critical density $\phi = 0.597$, we have system size 1024×1024 and quench was to $v_0 = 125$. (c) For critical density $\phi = 0.597$, system size was 256×256 and quench was to the critical $v_0 = 40/d_{\mathrm{BH}} \approx 36.14$.

was realized with 314 573 particles. To improve statistics we averaged over 10 independent runs each.

For quenches to the critical point [Fig. 2(c)] the final active velocity was set to $v_0 = 40/d_{\mathrm{BH}} \approx 36.14$ [17]. To study the scaling of the steady-state correlation length ξ_{max} with system size, different system sizes had to be realized. In particular, 100 independent runs for size 64×64 containing 2500 particles each, 50 runs for size 128×128 with 10 000 particles, and 15 runs for size 256×256 containing 40 401 particles each were performed.

B. Model and simulations: Active lattice systems

Quenches to the critical points were also performed for three active lattice models which are described in detail in Ref. [16]. In contrast to ABPs [17], these systems are already reported to exhibit steady-state critical exponents close to the 2D-Ising values [16]. From a computational point of view they are also less demanding, and superior statistics can be achieved in a straightforward implementation on CPUs.

Rotational diffusion and active propulsion are handled similarly to ABPs, but parameters are probabilities or rates in Monte Carlo (MC) simulations. Each particle can occupy a single site and is oriented toward one of its neighboring sites. Density is defined as the number of occupied divided by the total number of sites. Again, all simulations were performed with a fixed number of particles in 2D with periodic boundary conditions. One Monte Carlo time unit consists of as many individual Monte Carlo attempts as there are lattice spaces in the system. A rotation move only changes the orientation of the particle. In a translation move, a particle attempts to move to a neighboring site, which is always accepted if the targeted space is empty and rejected otherwise. To implement activity, movements along the particles' orientation were chosen with higher probability. Other directions were also allowed with reduced probability to account for translational diffusion.

As in Ref. [16] Model I [15] on a hexagonal (hex.) and a square (sq.) lattice were investigated to study the influence of lattice geometry on emerging dynamical properties. In each simulation step, the program attempts to change the orientation of a particle first: A Gaussian distributed random number (having standard deviation σ_{rot} and zero mean) is chosen and rounded to the nearest integer. The current orientation is adjusted by that integer, and the move is accepted with probability 1. As indicated, the rotational diffusion parameter σ_{rot} governs the width of the Gaussian distribution and hence the activity of the model: A low value for σ_{rot} corresponds to a low probability for orientation adjustments and thus enhanced activity and vice versa. Afterwards, a translation move is attempted with the same particle and accepted if the destination location is empty. The direction for the move is chosen at random, with probability w_+ along the particle's current orientation and with probability w_t for any of the remaining directions. For the hexagonal lattice probabilities are set to $w_+ = 25/30$ and $w_t = 1/30$ [15], for the square lattice $w_+ = 17/20$ and $w_t = 1/20$ [16].

In Model II [14] either a rotation or a translation move is attempted in an individual simulation step on the square lattice. A clockwise or anticlockwise rotation is performed with rate $w_1 = 0.1$, an attempted move along the current orientation is undertaken with rate w_+ and in any other direction with $w_t = 1$. Activity is regulated by adjusting w_+. Probabilities for each move are obtained by dividing the individual rates by the sum of all rates, namely $(w_+ + 3w_t + 2w_1)$. For a more in-depth discussion of the lattice models including steady state critical exponents and visualizations of particle moves, the reader is referred to Ref. [16]. Note that model parameters for the three active lattice models (including w_+, w_t, and w_1) were all taken from the original publications in which the models were first introduced [14–16]. In general, parameters were chosen to balance active movement with regular diffusion and mimic off-lattice models such as active Brownian particles. Such choices are helpful in dealing with matters that are parts of debates.

All lattice systems were equilibrated at the corresponding critical densities (0.524 for Model I hex., 0.498 for Model I sq., and 0.527 for Model II [16]) for 5000 time units in a mixed state and then quenched to the critical points. For equilibration, activity in Model I was set to $\sigma_{\mathrm{rot}} = 1$ and in Model II to $w_+ = 1.25$. Two hundred independent runs were performed for $L = 512$. The system size for the hexagonal lattice was increased by $2/\sqrt{3}$ to 592 in one direction to account for the hexagonal structure. Quenches to the critical points were simulated for five different system sizes. Four hundred independent runs were undertaken for $L = 64$ and $L = 128\,200$ runs for $L = 256$ and 512 and 50 for $L = 1024$. For the hexagonal lattices, one dimension was again adjusted as described above. Critical simulation parameters were taken from Ref. [16] as $\sigma_{\mathrm{rot}} = 0.3048$ for Model I hex., $\sigma_{\mathrm{rot}} = 0.2415$ for Model I sq. and $w_+ = 4.76$ for Model II sq.

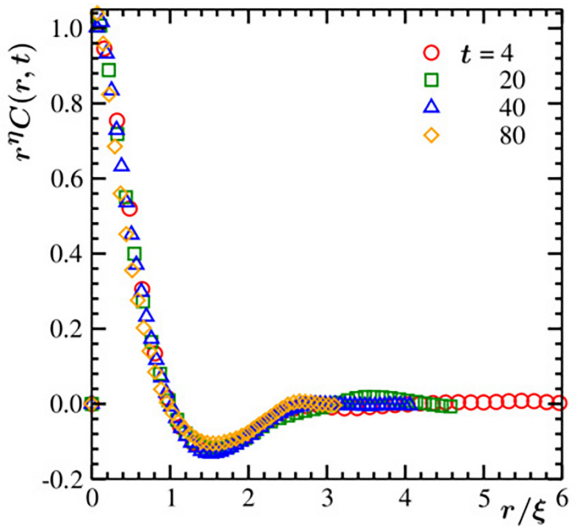

FIG. 3. Scaling plots of the correlation functions for the quench protocol of Fig. 2(c). Data from several different times are included for quenches of random initial configurations to the critical point, for the off-lattice model. The exponent η is set to 0.25, the 2D Ising value.

III. RESULTS AND DISCUSSION

As already stated, in Fig. 1 we show the phase diagram of the off-lattice model. The MIPS phase behavior resembles that of a vapor-liquid phase separation in passive systems rather closely. Nevertheless, it is not clear yet whether the critical behavior can be attributed to the Ising universality class. On the one hand, a study with the model used in this paper showed clear deviations from the 2D Ising universality class [17]. On the other hand, studies using other (somewhat similar) models concluded agreement with 2D Ising universality class [15,19] which resulted in a controversy. Recently, however, renormalization group studies of active matter models appeared [18,20] which could potentially reconcile these discrepancies and explain deviations from ideal Ising behavior. Apart from the Wilson-Fisher fixed point associated with the Ising universality, these studies find other points that limit the region in which the former dictates the phase transition. Even though little is known about the transitions described by these other points, they might potentially be connected to various forms of microphase separation observed, e.g., in Ref. [44].

In Fig. 2 we show snapshots from the evolution of our off-lattice ABP model system following a quench of random initial configurations to various state points. There, locations of particles are marked by dots. The frames under Figs. 2(a) and 2(b) are for quenches to state points inside the coexistence region (see Fig. 1). In Fig. 2(a) the overall density of particles is closer to the vapor branch of the coexistence curve. For this case, as expected, we observe formation and growth of disconnected clusters. In Fig. 2(b) we have included evolution snapshots corresponding to the critical value of $\phi = \phi_c$. In this case we observe an essentially bicontinuous structure. The snapshots in Fig. 2(c) are for quenches to the critical point, and the resulting fractal nature of the morphology can be appreciated. In the following we will only discuss Figs. 2(b) and 2(c) before moving to results from the lattice models.

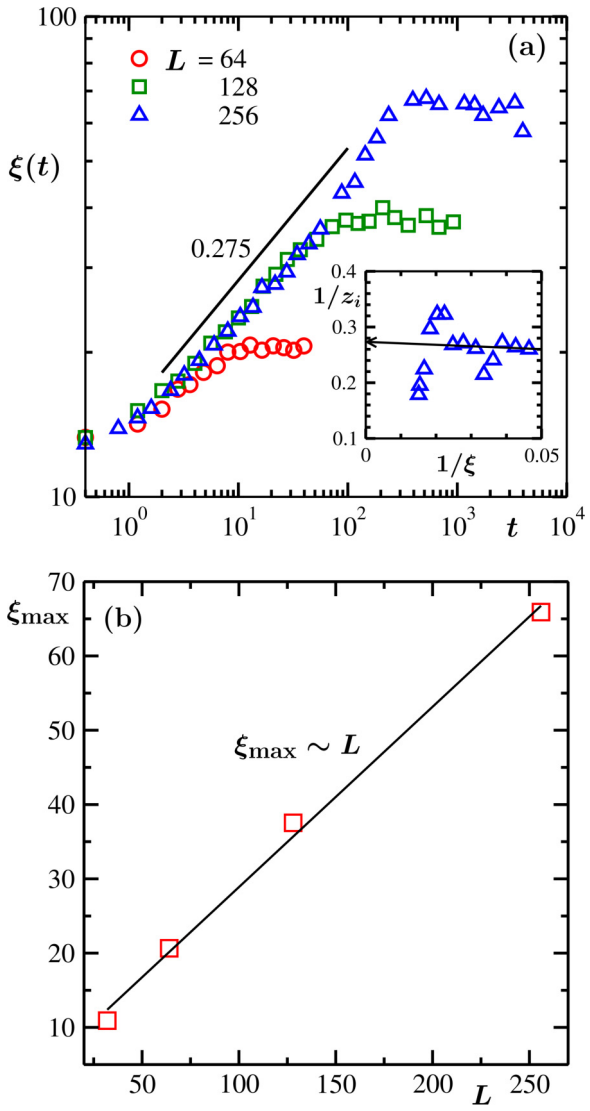

FIG. 4. (a) Results for growing correlation length are shown from different system sizes for quenches of random initial configurations to the critical point. The solid line is a power law, the value of the exponent mentioned next to it. Inset shows the plot of instantaneous exponent, $1/z_i$, as a function of $1/\xi$, for $L = 256$. (b) The steady state values of the correlation length, ξ_{max}, are plotted versus the system size L. These results are for the continuum model.

Note that in the case of Fig. 2(a), gathering meaningful data would require simulations of very large systems over long periods.

First we discuss the case of a quench to the critical point. In this case, due to the fractal nature of the structure the scaling property of Eq. (3) should be written as

$$C(r,t) \equiv r^{\Delta}\tilde{C}[r/\xi(t)], \tag{8}$$

where Δ is a function of the space and the fractal dimensions. Recalling that the equilibrium (here steady-state) correlation function in the critical vicinity has the form [38,39]

$$r^{-p}e^{-r/\xi};\ p = d - 2 + \eta, \tag{9}$$

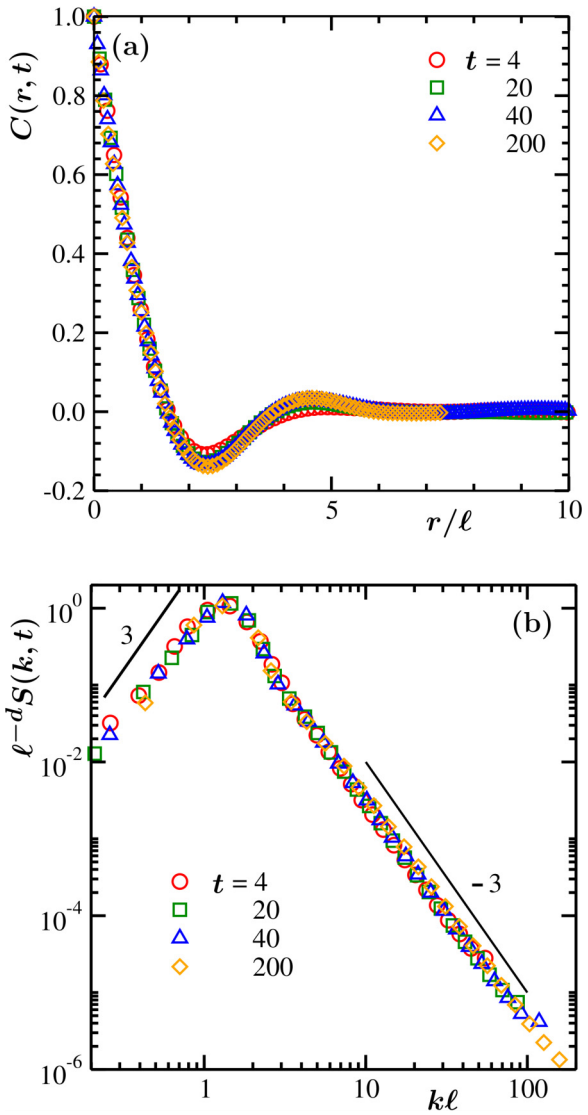

FIG. 5. Scaling plots of (a) $C(r,t)$ and (b) $S(k,t)$, for the quenching protocol described in Fig. 2(b). In panel (b) the solid lines represent power laws with exponent values mentioned in adjacent locations. These results are from the simulations of the off-lattice model.

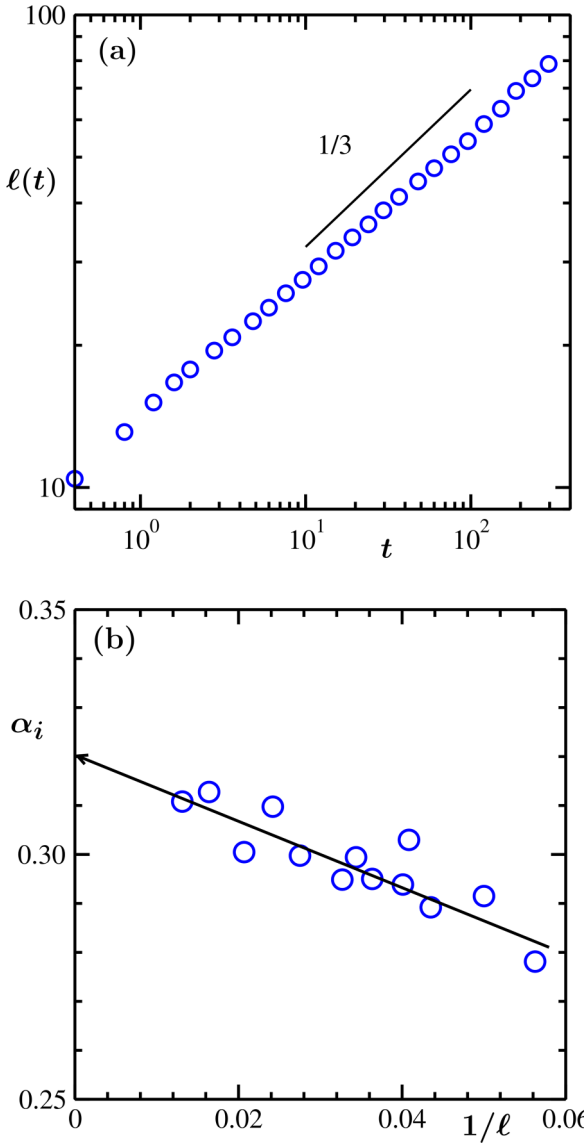

FIG. 6. (a) Plot of the average domain length as a function of time for the quenching protocol described in Fig. 2(b). (b) Instantaneous exponent corresponding to the growth in panel (a) is plotted versus $1/\ell$. These results are from the simulations of the continuum model.

we have the modified scaling form

$$r^{\eta}C(r,t) \equiv \tilde{C}[r/\xi(t)], \tag{10}$$

the critical exponent η being $1/4$ in space dimension $d = 2$ for the Ising class [39]. To confirm this scaling property we have plotted $r^{0.25}C(r,t)$ as a function of $r/\xi(t)$ in Fig. 3. Results from several different times have been included. Similar exercises were performed by replacing η by other numbers. The collapse for 0.25 appears the best.

The values of $\xi(t)$ obtained via the above discussed scaling analysis are plotted in Fig. 4(a), as a function of t. Data from different system sizes, as seen on the log-log scale, indicate a power-law growth with the exponent $\simeq 0.275$. This is consistent with $1/z$, with $z = 4 - \eta$, as expected for the 2D Ising class. In the inset we have shown the instantaneous exponent [46–48]

$$1/z_i = \frac{d\ln\xi(t)}{d\ln t}, \tag{11}$$

as a function of $1/\xi(t)$. Asymptotically, a convergence toward 0.275 can be appreciated. In Fig. 4(b) we demonstrate that the maximum correlation length scales with the system size, as in the passive case, at the critical point. A more accurate study calls for an exercise where $\xi_{\max}$ for different system sizes L are calculated at the finite-size critical points. Now we discuss the case of Fig. 2(b).

To check for the self-similar nature of the evolving pattern we calculate $C(r,t)$. Scaling plots of this quantity are presented in Fig. 5(a). In this case we aim to validate the scaling form of Eq. (3). Data from a few different times

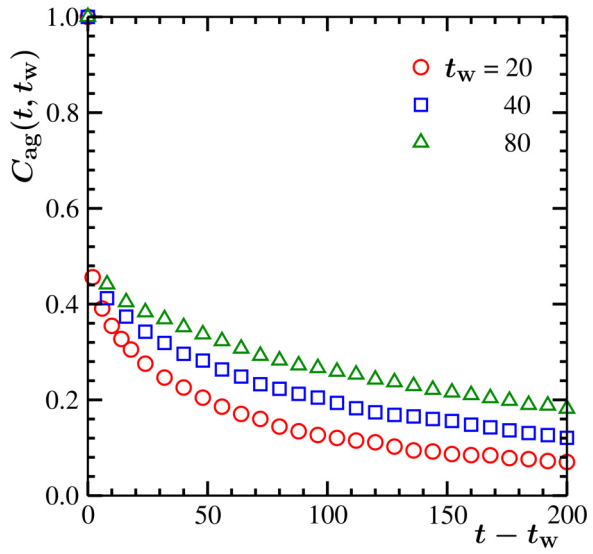

FIG. 7. Autocorrelation functions from the simulations of the off-lattice model are plotted versus the translated time $t - t_w$, for a few values of the waiting time t_w. These results are for the protocol of Fig. 2(b).

are shown. There, the distance axis is scaled by the average domain lengths at the corresponding times. Clearly, data from different times nicely collapse on top of each other, confirming self-similar growth. A scaling plot for the structure factor is presented in Fig. 5(b). There the power-law decay in the large wave vector (k) limit validates the Porod law [49]. The latter originates from scattering from sharp interfaces. We will discuss the small k power-law behavior later. Note that the presented scaling form for the structure factor $S(k, t)$ is a direct consequence of the fact that this quantity is the Fourier transform of $C(r, t)$.

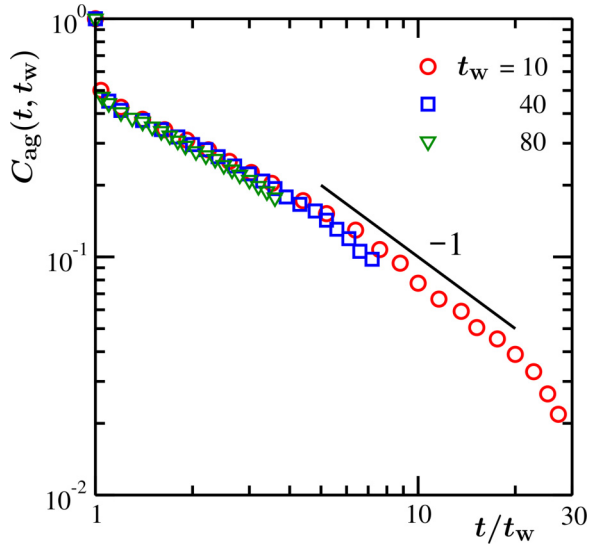

FIG. 8. Same as Fig. 7 but here we show $C_{ag}(t, t_w)$ as a function of t/t_w. The solid line has a power-law decay. The value of the exponent is mentioned next to the line.

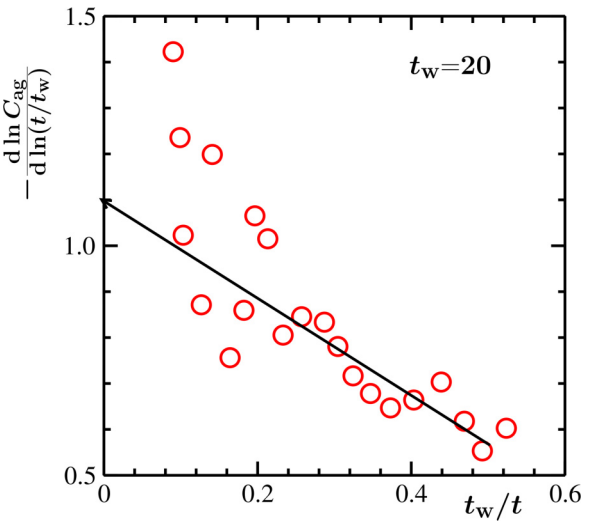

FIG. 9. The instantaneous aging exponent is plotted versus t_w/t for a value of t_w. The solid line is a guide to the eyes.

The average domain lengths are plotted in Fig. 6(a) as a function of time. The late time behavior is consistent with a power-law exponent 1/3. The latter is expected for diffusive domain growth as seen in Lifshitz-Slyozov mechanism [35] and is realized in Monte Carlo simulations [29] of Ising model via Kawasaki exchange [50] kinetics that preserves the system integrated order parameter over time [23,29]. In Fig. 6(b) we show [46–48]

$$\alpha_i = \frac{d \ln \ell(t)}{d \ln t}, \tag{12}$$

versus $1/\ell$. Clearly the asymptotic convergence ($\ell = \infty$ limit) is toward a value very close to 1/3.

In Fig. 7 we present the autocorrelation function, $C_{ag}(t, t_w)$, versus the translated time $t - t_w$. Clearly, results from different t_w do not overlap, as expected for evolving systems. The same data sets are plotted versus t/t_w in Fig. 8. Good overlap is observed. There the deviations of the data points from the master curve, that occur at different abscissa values for different t_w, are due to finite size of the systems. These departures should not be considered while quantifying the decay in the thermodynamically large system size limit. At large values of t/t_w, prior to the appearance of the finite-size effects, it appears that C_{ag} decays in a power-law manner with an exponent 1. For an accurate estimate of the exponent, in Fig. 9 we show the corresponding instantaneous exponent [32,36] $-d \ln C_{ag}/d \ln(t/t_w)$ as a function of t_w/t. The convergence is toward 1.1, when analyzed by discarding the finite-size affected part, that appears when t_w/t is small. This implies $\lambda \simeq 3.3$ which is in agreement with the Ising value for conserved order parameter [36].

Depending upon the conservation of order-parameter during evolution, there exist important bounds on the aging exponent λ [32,34]. For nonconserved order-parameter dynamics, which is not relevant to the present problem, Fisher and Huse provided a lower bound, $\lambda \geqslant d/2$, that can be obtained from the well-known Ohta-Jasnow-Kawasaki (OJK) correlation function [52] involving two space points and two times. Later Yeung, Rao, and Desai (YRD) [34] provided a

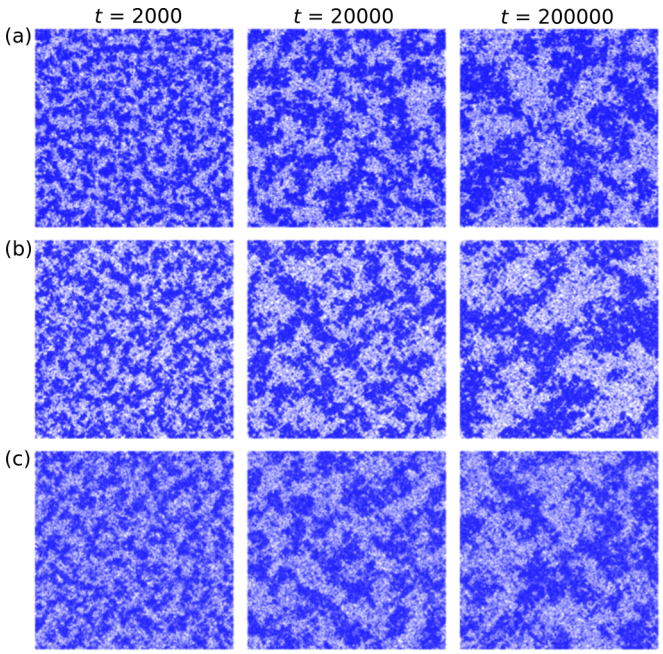

FIG. 10. Snapshots obtained during the evolutions of the considered lattice models are presented for three different times after the quenches to the critical points took place. Time t is given in Monte Carlo steps. The locations of the particles are marked. (a) For Model I hex., a system at critical density 0.524, is quenched to $\sigma_{\rm rot} = 0.3048$. The system is of size 512×592, to adjust for the hexagonal lattice structure. (b) For Model I sq., a critical density (0.498) system is quenched to $\sigma_{\rm rot} = 0.2415$. The system is of size 512×512. (c) For Model II sq., a system with critical density 0.527 is quenched to $w_+ = 4.76$. System is of size 512×512. The comparison of the results with the 2D conserved Ising model is presented in Fig. S4, in the Supplemental Material [45].

more general lower bound, viz.,

$$\lambda \geqslant \frac{d+\beta}{2}, \tag{13}$$

where β is the exponent characterizing the small wave-vector (k) power-law behavior [51],

$$S(k, t_w) \sim k^{\beta}. \tag{14}$$

For Ising-type systems, for standard nonconserved dynamics [36,52] $\beta = 0$. Thus, the YRD bound matches with the lower bound of FH. However, for similar models with conserved order-parameter dynamics one should ideally have [51] $\beta = 4$. The latter type of dynamics is of relevance here [23,29]. In Fig. 5(b) we have shown a representative plot of the structure factor, as a function of k, on a double-log scale. The small k behavior is consistent with $\beta = 3$. In that case we have the YRD bound to be equal to 2.5, recalling that here $d = 2$. Our result in Fig. 9 satisfies the lower bound of YRD. Somewhat smaller value of β than 4 was realized in earlier works also [53].

Before concluding, we present results from growth in the lattice models. In Fig. 10 we show evolution snapshots for quenches to the critical points for different lattice models. In Fig. 11 we have shown the growth of ξ for these lattice models. The results are consistent with the Ising case. For

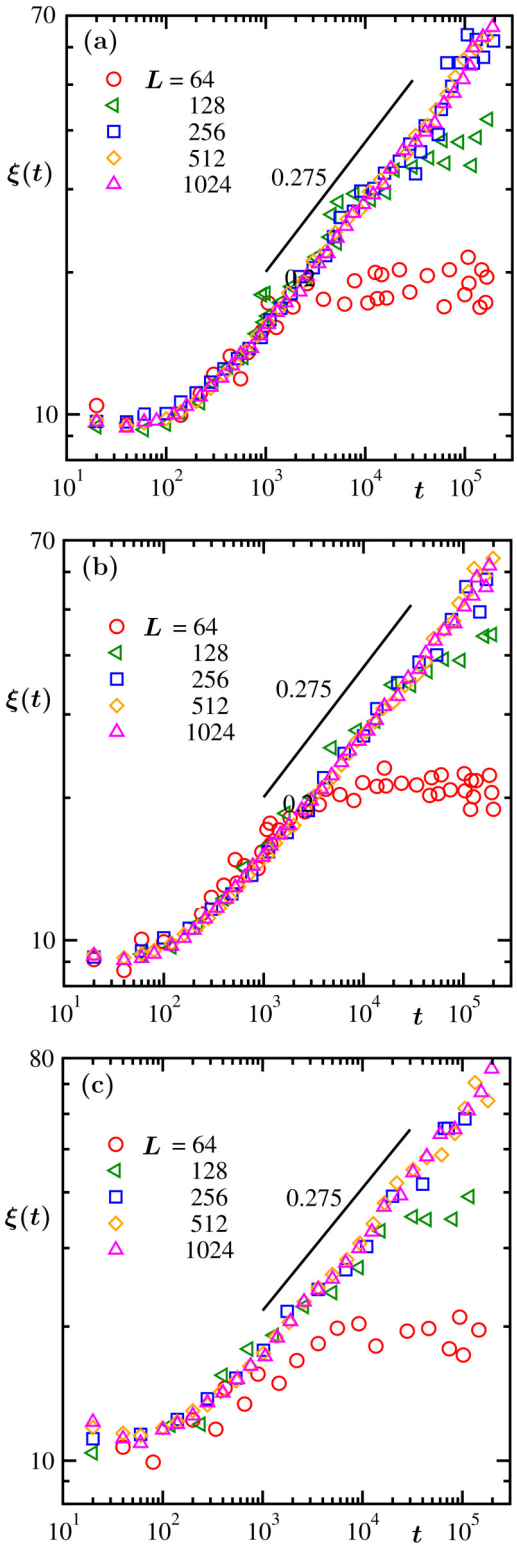

FIG. 11. Time-dependent correlation lengths are plotted for (a) square lattice using method-I, (b) hexagonal lattice using method-I, and (c) square lattice using method-II. The solid lines are power laws with mentioned value of the exponent. These results are for quenches of random initial configurations to the critical points.

quenches inside the coexistence regions, patterns obtained from the lattice models differ from the 2D conserved Ising model, and in the late stages the underlying lattice geometry becomes apparent. See Figs. S1 and S2 in the Supplemental Material [45]. The average domain length grows faster as well (Fig. S3) [45]. Further investigations, thus, are certainly warranted.

IV. CONCLUSION

We have studied critical and off-critical kinetics of vapor-liquid phase transition in a model system consisting of active Brownian particles [17]. Results are presented for structure, growth, and aging. Each of these aspects appear to be quite similar to those observed during phase separation in the Ising model with conserved order-parameter dynamics [23,29]. The growth of average domain size follows a power-law behavior with an exponent $\alpha = 1/3$, as expected for Lifshitz-Slyzov mechanism [35]. The aging exponent λ appears to have a value 3.3 that is in quite good agreement with two-dimensional conserved dynamics of Ising model [36] within 10%. The value of λ satisfies the Yeung-Rao-Desai bound [34]. The structure also matches Ising behavior.

Note that our results for ABPs are not necessarily in contradiction to the central claim of Ref. [17], namely that static critical exponents differ from the 2D Ising case. In our opinion, they merely indicate that critical behavior in nonequilibrium systems may still not be as well-understood as in the equilibrium case, and that future research in this field is certainly warranted. On a related note, inertia [54,55] and hydrodynamics [56] also appear to affect behavior of active particles in the phase separated region and beyond, and a thorough investigation of their influence on dynamics, particularly in the critical region would be interesting as well.

Finally, we have also presented results from a few lattice models [15] for quenches to the critical points. In these cases also the structure and dynamics, like in the case of the continuum model, are similar to those for the conserved Ising model in $d = 2$.

ACKNOWLEDGMENTS

F.D. and P.V. gratefully acknowledge financial support by the Deutsche Forschungsgemeinschaft within priority program SPP 1726 (Grant No. VI 237/5-2) and through Project No. 233630050-TRR 146. F.D. and P.V. acknowledge the Zentrum für Datenverarbeitung, Mainz for computing time on the MOGON II cluster. S.K.D. acknowledges hospitality during scientific visits in University of Mainz and partial support from JNCASR. Stimulating discussions with Thomas Speck are gratefully acknowledged.

[1] T. Vicsek and A. Zafeiris, Phys. Rep. **517**, 71 (2012).
[2] C. Bechinger, R. Di Leonardo, H. Löwen, C. Reichhardt, G. Volpe, and G. Volpe, Rev. Mod. Phys. **88**, 045006 (2016).
[3] G. Gompper, R. G. Winkler, T. Speck, A. Solon, C. Nardini, F. Peruani, H. Loewen, R. Golestanian, U. B. Kaupp, L. Alvarez, T. Kioerboe, E. Lauga, W. Poon, A. D. Simone, F. Cichos, A. Fischer, S. M. Landin, N. Soeker, R. Kapral, P. Gaspard *et al.*, J. Phys.: Condens. Matter **32**, 193001 (2020).
[4] M. E. Cates and J. Tailleur, Annu. Rev. Condens. Matter Phys. **6**, 219 (2015).
[5] Y. Fily and M. C. Marchetti, Phys. Rev. Lett. **108**, 235702 (2012).
[6] G. S. Redner, M. F. Hagan, and A. Baskaran, Phys. Rev. Lett. **110**, 055701 (2013).
[7] J. Stenhammar, A. Tiribocchi, R. J. Allen, D. Marenduzzo, and M. E. Cates, Phys. Rev. Lett. **111**, 145702 (2013).
[8] J. Stenhammar, D. Marenduzzo, R. J. Allen, and M. E. Cates, Soft Matter **10**, 1489 (2014).
[9] A. Wysocki, R. G. Winkler, and G. Gompper, Europhys. Lett. **105**, 48004 (2014).
[10] J. Bialké, T. Speck, and H. Löwen, J. Non-Cryst. Solids **407**, 367 (2015).
[11] J. T. Siebert, J. Letz, T. Speck, and P. Virnau, Soft Matter **13**, 1020 (2017).
[12] P. Digregorio, D. Levis, A. Suma, L. F. Cugliandolo, G. Gonnella, and I. Pagonabarraga, Phys. Rev. Lett. **121**, 098003 (2018).
[13] L. Caprini, U. M. B. Marconi, C. Maggi, M. Paoluzzi, and A. Puglisi, Phys. Rev. Res. **2**, 023321 (2020).
[14] S. Whitelam, K. Klymko, and D. Mandal, J. Chem. Phys. **148**, 154902 (2018).
[15] B. Partridge and C. F. Lee, Phys. Rev. Lett. **123**, 068002 (2019).
[16] F. Dittrich, T. Speck, and P. Virnau, Eur. Phys. J. E **44**, 53 (2021).
[17] J. T. Siebert, F. Dittrich, F. Schmid, K. Binder, T. Speck, and P. Virnau, Phys. Rev. E **98**, 030601(R) (2018).
[18] F. Caballero, C. Nardini, and M. E. Cates, J. Stat. Mech. (2018) 123208.
[19] C. Maggi, M. Paoluzzi, A. Crisanti, E. Zaccarelli, and N. Gnan, Soft Matter **17**, 3807 (2021).
[20] T. Speck, Phys. Rev. E **105**, 064601 (2022).
[21] C. Maggi, N. Gnan, M. Paoluzzi, E. Zaccarelli, and A. Crisanti, Comm. Phys. **5**, 55 (2022).
[22] N. Gnan and C. Maggi, Soft Matter **18**, 7654 (2022).
[23] A. J. Bray, Adv. Phys. **51**, 481 (2002).
[24] V. Wadhawan and S. E. Puri, *Kinetics of Phase Transitions*, 1st ed. (CRC Press, Boca Raton, FL, 2009)
[25] P. Cremer and H. Löwen, Phys. Rev. E **89**, 022307 (2014).
[26] S. K. Das, J. Chem. Phys. **146**, 044902 (2017).
[27] K. Binder and P. Virnau, Soft Mater. **19**, 267 (2021).
[28] G. Grégoire and H. Chaté, Phys. Rev. Lett. **92**, 025702 (2004).
[29] D. P. Landau and K. Binder, *A Guide to Monte Carlo Simulations in Statistical Physics*, 2nd ed. (Cambridge University Press, Cambridge, UK, 2005).
[30] S. Chakraborty and S. K. Das, J. Chem. Phys. **153**, 044905 (2020).
[31] S. Paul, A. Bera, and S. K. Das, Soft Matter **17**, 645 (2021).
[32] D. S. Fisher and D. A. Huse, Phys. Rev. B **38**, 373 (1988).
[33] F. Liu and G. F. Mazenko, Phys. Rev. B **44**, 9185 (1991).
[34] C. Yeung, M. Rao, and R. C. Desai, Phys. Rev. E **53**, 3073 (1996).
[35] I. Lifshitz and V. Slyozov, J. Phys. Chem. Solids **19**, 35 (1961).

[36] J. Midya, S. Majumder, and S. K. Das, Phys. Rev. E **92**, 022124 (2015).
[37] P. C. Hohenberg and B. I. Halperin, Rev. Mod. Phys. **49**, 435 (1977).
[38] A. Onuki, *Phase Transition Dynamics* (Cambridge University Press, Cambridge, UK, 2002).
[39] M. E. Fisher, Rep. Prog. Phys. **30**, 615 (1967).
[40] S. K. Das, S. A. Egorov, B. Trefz, P. Virnau, and K. Binder, Phys. Rev. Lett. **112**, 198301 (2014).
[41] B. Trefz, S. K. Das, S. A. Egorov, P. Virnau, and K. Binder, J. Chem. Phys. **144**, 144902 (2016).
[42] J. A. Anderson, J. Glaser, and S. C. Glotzer, Comput. Mater. Sci. **173**, 109363 (2020).
[43] I. Buttinoni, J. Bialké, F. Kümmel, H. Löwen, C. Bechinger, and T. Speck, Phys. Rev. Lett. **110**, 238301 (2013).
[44] E. Tjhung, C. Nardini, and M. E. Cates, Phys. Rev. X **8**, 031080 (2018).
[45] See Supplemental Material at http://link.aps.org/supplemental/10.1103/PhysRevE.108.024609 for detailed results (Figs. S1–S4) on the active lattice models and their comparison with two-dimensional Ising model with conserved order-parameter dynamics.
[46] D. A. Huse, Phys. Rev. B **34**, 7845 (1986).
[47] J. G. Amar, F. E. Sullivan, and R. D. Mountain, Phys. Rev. B **37**, 196 (1988).
[48] S. Majumder and S. K. Das, Phys. Rev. E **84**, 021110 (2011).
[49] G. Porod, *Small-angle X-ray Scattering*, edited by O. Glatter and O. Kratky (Academic Press, New York, NY, 1982).
[50] K. Kawasaki, *Phase Transitions and Critical Phenomena*, Vol. 2, edited by C. Domb and M. S. Green (Academic Press, New York, NY, 1972), p. 443.
[51] C. Yeung, Phys. Rev. Lett. **61**, 1135 (1988).
[52] T. Ohta, D. Jasnow, and K. Kawasaki, Phys. Rev. Lett. **49**, 1223 (1982).
[53] S. Ahmad, S. K. Das, and S. Puri, Phys. Rev. E **85**, 031140 (2012).
[54] H. Löwen, J. Chem. Phys. **152**, 040901 (2020).
[55] L. Caprini and U. Marini Bettolo Marconi, J. Chem. Phys. **154**, 024902 (2021).
[56] G. Negro, C. B. Caporusso, P. Digregorio, G. Gonnella, A. Lamura, and A. Suma, Eur. Phys. J. E **45**, 75 (2022).